Published in final edited form as:
Acad Radiol. 2013 January ; 20(1): 115–121. doi:10.1016/j.acra.2012.07.011.

Comparison of Semi-automatic Volumetric VX2 Hepatic Tumor Segmentation from Cone Beam CT and Multi-detector CT with Histology in Rabbit Models

Olivier Pellerin, MD, MSc, **MingDe Lin, PhD**, **Nikhil Bhagat, MD**, **Roberto Ardon, PhD**, **Benoit Mory, PhD**, and **Jean-François Geschwind, MD**
Russell H. Morgan Department of Radiology and Radiological Science, Division of Vascular and Interventional Radiology, Johns Hopkins Hospital, Sheikh Zayed Tower, Suite 7203, 1800 Orleans Street, Baltimore, MD 21287 (O.P., N.B., J.-F.G.); Clinical Informatics, Interventional, and Translational Solutions, Philips Research North America, Briarcliff Manor, New York (M.L.); and Philips Healthcare, Suresnes, France (R.A., B.M.)

Abstract

Rationale and Objectives—The purpose of this study was to compare tumor volume in a VX2 rabbit model as calculated using semiautomatic tumor segmentation from C-arm cone-beam computed tomography (CBCT) and multidetector computed tomography (MDCT) to the actual tumor volume.

Materials and Methods—Twenty VX2 tumors in 20 adult male New Zealand rabbits (one tumor per rabbit) were imaged with CBCT (using an intra-arterial contrast medium injection) and MDCT (using an intravenous contrast injection). All tumor volumes were measured using semiautomatic three-dimensional volumetric segmentation software. The software uses a region-growing method using non-Euclidean radial basis functions. After imaging, the tumors were excised for pathologic volume measurement. The imaging-based tumor volume measurements were compared to the pathologic volumes using linear regression, with Pearson's test, and correlated using Bland-Altman analysis.

Results—Average tumor volumes were 3.5 ± 1.6 cm^3 (range, 1.4–7.2 cm^3) on pathology, 3.8 ± 1.6 cm^3 (range, 1.3–7.3 cm^3) on CBCT, and 3.9 ± 1.6 (range, 1.8–7.5 cm^3) on MDCT ($P < .001$). A strong correlation between volumes on pathology and CBCT and also with MDCT was observed (Pearson's correlation coefficient = 0.993 and 0.996, $P < .001$, for CBCT and MDCT, respectively). Bland-Altman analysis showed that MDCT tended to overestimate tumor volume, and there was stronger agreement for tumor volume between CBCT and pathology than with MDCT, possibly because of the intra-arterial contrast injection.

Conclusions—Tumor volume as measured using semiautomatic tumor segmentation software showed a strong correlation with the "real volume" measured on pathology. The segmentation software on CBCT and MDCT can be a useful tool for volumetric hepatic tumor assessment.

Keywords

Tumor segmentation software; C-arm cone-beam CT; multidetector CT; VX2 hepatic tumor

Address correspondence to: J.-F.G. jfg@jhmi.edu.

A change in tumor volume as a response to local therapy such as transcatheter arterial chemoembolization is a prognostic indicator of therapeutic success. Tumor size is the only component of the Response Evaluation Criteria in Solid Tumors (RECIST) (1). First described in 2000, RECIST is based on tumor diameter measurement, in which the longest diameter of a given target lesion, or the sum of the longest diameters for a set of target lesions, is measured and compared before and after chemoembolization on cross-sectional imaging (either computed tomography or magnetic resonance imaging. It is a one-dimensional measurement that often poorly represents true tumor response after chemoembolization and is subject to high interobserver variability (2,3). Although RECIST was appropriate at the time of its introduction, the simplicity of RECIST now makes insufficient use of the sophisticated advances in modern imaging units. With the advent of multidetector computed tomography (MDCT) and improved detectors, the ability to assess tumor volume using three-dimensional (3D) metrics has become much more feasible. Furthermore, with the advent of C-arm cone-beam computed tomography (CBCT), tumors can be assessed during the procedure for planning or for efficacy of treatment (4). However, before volume-based metrics can supplant RECIST, these methods must be shown to be accurate and precise. This was recognized in version 1.1 of RECIST (released in 2009): the importance of studying volumetric anatomic assessment in greater detail is necessary before anatomic unidimensional assessment of tumor burden can be abandoned (1).

The purpose of this study was to evaluate the accuracy of semiautomatic tumor segmentation software with CBCT and MDCT and compare these measurements to pathologic volume-based measurements in a VX2 rabbit hepatic tumor model.

MATERIALS AND METHODS

This study was an ancillary study. The aim of the primary study was to explore the performance of drug-eluting beads in terms of tumor penetration and pharmacokinetics. All animal studies were approved by our institution’s animal care and use committee. All procedures were conducted under their guidelines.

Animals

Twenty adult male New Zealand white rabbits weighing between 3.8 and 4.3 kg (Myrtle’s Rabbitry, Thompson Station, TN) were used for this study. All rabbits were implanted with VX2 liver tumors, as described in previous work (5). These animals were used for another study (doxorubicin-eluting bead treatment).

Anesthesia

The tumor-bearing animals were anesthetized twice: once for tumor implantation and once for tumor treatment. For tumor implantation, induction was achieved with 5% isoflurane (Hospira, Lake Forest, IL) and 95% oxygen (Air Gas, Salem, NH) and then sustained with 2.5% isoflurane and 97.5% oxygen. For treatment, the animals were premedicated with an intramuscular injection of acepromazine (2.5 mg/kg; Phoenix, St Joseph, MO) and ketamine hydrochloride (Ketaject 44 mg/kg; Phoenix). Sedation was maintained with propofol 10 mg/mL (APP Pharmaceuticals, Schaumburg, IL) in monitored boluses of 2 mg (0.25 mL) intravenously via the right marginal ear vein. After the procedure, analgesic buprenorphine (0.02–0.05 mg/kg) was injected intramuscularly for pain relief.

MDCT

All animals underwent multidetector biphasic computed tomographic scans before the embolization and treatment procedure, which was 7 days after tumor implantation. At 7 days, the aggressively growing VX2 tumors were close to spherical in shape and without

necrotic cores as seen in larger sized tumors (>3 cm in diameter). This was required for the primary study. Imaging was performed using a conventional multidetector computed tomographic unit (Toshiba Aquilion ONE; Toshiba Corporation, Tokyo, Japan). MDCT was performed using tube voltage of 120 kVp and tube current of 80 mA, a rotation time of 0.5 seconds, and a scan time of 60.5 seconds. The matrix used was 512 × 512 × 200, with a 492 × 492 × 192 mm reconstructed field of view. The arterial and portal acquisitions were respectively performed at 12 and 30 seconds after contrast injection (2 ml Oxilan 300 mg I/mL; Guerbet LLC, Roissy, France).

Drug-eluting Bead Transarterial Chemoembolization (DEB-TACE) Procedure

For all rabbits, an incision was made in the skin and subcutaneous structures after shaving, disinfecting, and draping the right inner thigh and groin. Blunt dissection was performed to expose the right femoral artery. A 3-F introducer (Check-Flo; Cook, Bloomington, IN) was introduced over a guide wire through the femoral arterial access. Next, the hepatic artery was catheterized using a 2-F JB1 catheter (Cook) and a 0.014-inch guide wire (Transend; Boston Scientific Corporation, Miami, FL). Chemoembolization was performed using 100 to 300 μm drug-eluting beads (LC Beads; Biocompatibles, Oxford, CT) loaded with doxorubicin (these animals were used for another study, as described above).

C-arm CBCT

All animal imaging was performed using a commercial C-arm system (Allura FD20 with XperCToption; Philips Healthcare, Best, The Netherlands). C-arm CBCT was performed using tube voltage of 80 kVp, tube current of 85 mA, tube exposure time of 5 ms, with a 5-second scan time, and a frame rate of 60 frames/s. The images were reconstructed immediately after image acquisition using the commercially available 3D algorithm on the scanner to a 256 × 256 × 192 matrix with a voxel size of 0.98 mm^3. All cone-beam computed tomographic images were acquired before embolization with a simultaneous contrast injection (2 ml Oxilan 300 mg I/mL).

Animal Sacrifice, Histology, and Tumor Volume Measurement

All animals were sacrificed under deep anesthesia by intravenous injection of 100 mg/kg intravenous thiopental 7 days after the DEB-TACE procedure. Necropsy was done on all animals. Rabbit livers were dissected, carefully removed, and placed in a container containing 5% formaldehyde. Two weeks later, 5-mm tumor slices were taken for gross examination. Tumor shape was classified as an oblate or a prolate spheroid by the primary investigator. Tumor volume was calculated along the spheroid volume as $V = (\pi A^2 B)/6$. For prolate and oblate spheroids, the equatorial diameters were, respectively, A and B, and polar diameters were, respectively, B and A. The two diameters were carefully measured macroscopically with a caliper. Measurements were repeated two times in two separate blind and random sessions to minimize influence of previous results.

Semiautomatic Tumor Segmentation

Semiautomatic 3D volume segmentation using non-Euclidean radial basis functions was used by an interventional radiologist with 9 years of experience (O.P.) on the pre-DEB-TACE contrast-enhanced cone-beam and multidetector computed tomographic images to segment the tumors. Briefly, this method is inspired by non-Euclidean geometry and the theory of radial basis functions (mathematically, functions whose values depends only on the distance from the origin) (6). This method allows segmentations that follow 3D image features, including straight edges and corners. The algorithm used is based on the linear combination of image-dependent shapes. Each shape is built on the basis of image features located in a 3D region whose center and size are specified by the user (interactively, this

information is recovered by a mouse click followed by a mouse drag). The combination of the segmentation shape construction is done through the optimization of an image-based criterion (eg, maximizing the gradient flow through the boundary of the combination). Moreover, the user can constrain the algorithm to include or exclude a new segmentation shape (defined by a new point and size), thus freely controlling the final aspect of the global segmentation combination. This method was used because it can accurately segment in three dimensions with minimal user interaction. Segmentation time was recorded.

In practice, the user identifies an initial control point. From there, the user can interactively expand or contract the 3D region of interest. Additional segmentations can be included by placing more control points. Corrections are made in the same volumetric way. Tumor volume segmentation measurements were made two times in two separate blind and random sessions to minimize influence of previous results.

Statistical Analysis

Tumor volumes were measured with two different imaging modalities and were compared to pathology (as a gold standard) using linear regression, including Pearson's correlation coefficient. In addition to correlation analysis, Bland-Altman analyses were performed to evaluate the absolute agreement of the measurements between the different modalities (7). To directly compare the predictive performance of the various tests, a method as described by Sheiner and Beal was used (8). This method evaluates the predictive performance of a test by calculating the prediction error and the bias. Prediction error is an indicator of the precision of a test, while bias gives information about the systematic component of the prediction error. In other words, the bias reflects an underestimation or overestimation of a test. Furthermore, this method gives the opportunity to compare the performance of the different imaging modalities. Intraobserver variability was estimated with using an intraclass correlation coefficient and its 95% confidence interval. Statistical analyses were performed using Xlstat (Addinsoft, Paris, France).

RESULTS

All rabbit hepatic arteries were successfully catheterized. The presence of a hypertrophic tumor feeder vessel, associated with a hypervascular tumor stain, was observed in all rabbits (Fig 1a). Selective catheterization and DEB-TACE were possible in all rabbits, and drug-eluting beads were injected until there was five-beat stasis in the tumor-feeding vessel. Multidetector and cone-beam computed tomographic images were acquired before embolization. Semiautomatic tumor segmentation was performed retrospectively. The time it took to segment each of the 20 cone-beam computed tomographic examinations in the first and second reading sessions was 72 ± 28 seconds (range, 50–300 seconds) and 88 ± 34 seconds (range, 68–250 seconds), respectively ($P = .01$). Typically, five to nine mouse button clicks were needed to sufficiently segment a tumor. As seen in Figure 2, the segmented volumes matched the tumor boundaries very well.

Tumor diameters varied from 0.8 to 3.2 cm on pathologic examination (mean, 1.8 ± 0.5 cm; Fig 1b). Twelve tumors (60%) were classified as prolate spheroid in shape and eight (40%) as oblate spheroid in shape. The mean tumor volume was 3.5 ± 1.6 cm^3 (range, 1.4–7.2 cm^3) on pathology, 3.8 ± 1.6 cm^3 (range, 1.3–7.3 cm^3) on CBCT, and 3.9 ± 1.6 cm^3 (range, 1.8–7.5 cm^3) on MDCT ($P < .001$; Fig 2). Individual measurements are shown in Table 1.

The results of Pearson's correlation analyses are shown in Figure 3a and 3b. Measurements of tumor volume on CBCT showed a good correlation with pathology (Pearson' correlation coefficient = 0.993, $P < .001$). The correlation between MDCT and pathology was also strong (Pearson's correlation coefficient = 0.996, $P < .001$).

A comparative analysis using Bland-Altman plots (Fig 3c and 3d) showed that MDCT tended to overestimate tumor volume, reflected by a mean difference of 0.4 cm^3 with limits of agreement at 0.3 and 0.4 cm^3. This means that 95% of the diameters measured on MDCT lay within the range of 0.3 to 0.4 cm^3 from the true volume as measured in the pathologic specimens. The agreement between CBCT and pathology proved to be accurate, like that of MDCT. The mean difference was 0.3 cm^3 (limits of agreement, 0.2 and 0.3 cm^3).

The Sheiner and Beal test confirmed that the results were in line with the observations in the Bland-Altman plots: tumor volume segmentation on MDCT showed the highest precision (0.368) and the smallest bias (0.275), and this precision was significantly better than any other measurement in this study, as can be gathered from the 95% confidence intervals (Table 2).

Excellent intraobserver reproducibility was observed for the tumor volume measurement on the pathologic samples and on both modalities used in our study. Intraclass coefficients were 0.934, 0.951, and 0.958 for volumes on pathology, CBCT, and MDCT, respectively. Intraobserver reproducibility results are provided in Table 3.

DISCUSSION

This study demonstrates a strong correlation between true VX2 hepatic tumor volume (the gold standard being histologic measurements) and calculated volumes using semiautomatic tumor volume segmentation software. This was associated with excellent intraobserver reproducibility. To the extent of our knowledge, no previous experimental study comparing tumor volume segmentation software with macroscopic samples has been reported. Tumor burden and enhancement are important prognostic factors when discussing locoregional therapy. One-dimensional or two-dimensional measurements are routinely used to estimate tumor size for hepatocellular carcinoma staging and assessment of treatment response. Studies have found that tumor volumetry may be a more accurate standard than one-dimensional and two-dimensional measurements (9–11). However, RECIST is still used because of the absence of sufficient standardization and evidence to abandon anatomic assessment of tumor burden (1).

Tumor volume segmentation software is receiving increasing attention and research efforts from the medical imaging community. Some semiautomated methods, such as region growing, isocontour, active contour, watershed, and nonEuclidean radial basis functions, have been described (12–16). Region-growing algorithms are the most common approaches in use. Recently Zhou et al (17), in a benchmark study, showed good performance of region growing with knowledge-based constraints compared to Bayesian rule-based 3D region growing. The algorithm used herein is based on the linear combination of image-dependent shapes. Each shape is built on the basis of an image's features located in a 3D region whose center and size are specified by the user (interactively, this information is recovered by a mouse click followed by a mouse drag). The combination of these shapes is done through the optimization of an image-based criterion (eg, maximizing the gradient flow through the boundary of the combination). Moreover, the user can constrain the algorithm to include or exclude a new shape (defined by a new point and size), thus freely controlling the final aspect of the global combination. Manual segmentation requires a high level of expertise and incorporates an expert's knowledge with image features to make accurate segmentations. This semiautomatic method provides similar results but at only a fraction of user interaction time.

Tumor volume segmentation software needs to cope with difficulties stemming from the complex appearances of tumors, neighboring structures, variable degrees of enhancement,

and adjacent artifacts. In the present study, the tumor volume segmentation software was successfully used to segment tumors with two imaging modalities (CBCT and MDCT).

The small but significant difference observed in tumor volume measurements between pathology and the two imaging methods tested may be related to tumor shrinkage. Tumor shrinkage could have been caused by two independent factors. First, the pathologic examinations occurred 14 days after the imaging studies (CBCT and MDCT). In addition, there was an embolization procedure between the imaging and pathologic analyses. Because these particles typically induce necrosis, tumor volumes could have been affected by this procedure. However, we feel that minimal changes in volume would have occurred between these time points. Second, tumor volume measurement occurred after 2 weeks of formalin impregnation. Formalin impregnation induces tumor shrinkage in VX2 tumors because of their partial necrotic center. However, in human prostate cancer, linear correction factors for tumor shrinkage between 1.04 and 1.14 have been described, indicating that the influence of shrinkage might be rather low (18). In the present study, all tumors presented with small volumes. The partial volume effects associated with portal venous enhancement, and the low spatial resolution used in our protocol, may have a potential influence on tumor volume overestimation with MDCT.

Because of the ancillary nature of this study, the exact tumor volume could not be measured in a graduated cylinder. In a future study in which tumor volume measurement is the primary goal, a graduated cylinder measure could be done to provide even more accurate results.

CONCLUSIONS

To our knowledge, this is the first experimental study to confirm in a VX2 rabbit hepatic tumor model the accuracy of semiautomatic tumor volume segmentation software used on preprocedural CBCT and MDCT with pathologic validation. The volume as measured by the semiautomatic tumor segmentation software showed a strong correlation with the volume measured on pathology. Use of the segmentation software on CBCT and MDCT can be helpful for volumetric hepatic tumor assessment and can help interventional radiologists plan treatments by demonstrating the tumor shape, location, vascular feeding network, and residual tumor. Furthermore, this volumetric approach could also be a first step toward volume enhancement quantification to discriminate enhanced and non-enhanced portions of tumors to determine the sections that are viable (associating contrast enhancement with viability).

Acknowledgments

This study was funded by Société Française de Radiologie (Paris, France) and by grant R01 CA160771 from the National Cancer Institute (Bethesda, MD).

References

1. Eisenhauer EA, Therasse P, Bogaerts J, et al. New response evaluation criteria in solid tumours: revised RECIST guideline (version 1. 1). Eur J Cancer. 2009; 45:228–247. [PubMed: 19097774]
2. Lim HK, Han JK. Hepatocellular carcinoma: evaluation of therapeutic response to interventional procedures. Abdom Imaging. 2002; 27:168–179. [PubMed: 11847576]
3. Suzuki C, Torkzad MR, Jacobsson H, et al. Interobserver and intraobserver variability in the response evaluation of cancer therapy according to RECIST and WHO-criteria. Acta Oncol. 2010; 49:509–514. [PubMed: 20397778]
4. Loffroy R, Lin M, Rao P, et al. Comparing the detectability of hepatocellular carcinoma by C-arm dual-phase cone-beam computed tomography during hepatic arteriography with conventional

contrast-enhanced magnetic resonance imaging. Cardiovasc Intervent Radiol. 2012; 35:97–104. [PubMed: 21328023]

5. Lee KH, Liapi E, Buijs M, et al. Percutaneous US-guided implantation of Vx-2 carcinoma into rabbit liver: a comparison with open surgical method. J Surg Res. 2009; 155:94–99. [PubMed: 19181344]
6. Mory, B.; Ardon, R.; Yezzi, AJ., et al. Non-Euclidean image-adaptive radial basis functions for 3D interactive segmentation. 2009 IEEE 12th International Conference on Computer Vision 2009; Piscataway, NJ: IEEE; 2009. p. 787-794.
7. Bland JM, Altman DG. Statistical methods for assessing agreement between two methods of clinical measurement. Lancet. 1986; 1:307–310. [PubMed: 2868172]
8. Sheiner LB, Beal SL. Some suggestions for measuring predictive performance. J Pharmacokinet Biopharm. 1981; 9:503–512. [PubMed: 7310648]
9. Dachman AH, MacEneaney PM, Adedipe A, et al. Tumor size on computed tomography scans: is one measurement enough? Cancer. 2001; 91:555–560. [PubMed: 11169938]
10. Hopper KD, Kasales CJ, Eggli KD, et al. The impact of 2D versus 3D quantitation of tumor bulk determination on current methods of assessing response to treatment. J Comput Assist Tomogr. 1996; 20:930–937. [PubMed: 8933793]
11. Prasad SR, Jhaveri KS, Saini S, et al. CT tumor measurement for therapeutic response assessment: comparison of unidimensional, bidimensional, and volumetric techniques initial observations. Radiology. 2002; 225:416–419. [PubMed: 12409574]
12. Keil S, Behrendt FF, Stanzel S, et al. Semi-automated measurement of hyperdense, hypodense and heterogeneous hepatic metastasis on standard MDCT slices. Comparison of semi-automated and manual measurement of RECIST and WHO criteria. Eur Radiol. 2008; 18:2456–2465. [PubMed: 18523775]
13. Mahr A, Levegrun S, Bahner ML, et al. Usability of semiautomatic segmentation algorithms for tumor volume determination. Invest Radiol. 1999; 34:143–150. [PubMed: 9951794]
14. Ray S, Hagge R, Gillen M, et al. Comparison of two-dimensional and three-dimensional iterative watershed segmentation methods in hepatic tumor volumetrics. Med Phys. 2008; 35:5869–5881. [PubMed: 19175143]
15. Yim PJ, Vora AV, Raghavan D, et al. Volumetric analysis of liver metastases in computed tomography with the fuzzy C-means algorithm. J Comput Assist Tomogr. 2006; 30:212–220. [PubMed: 16628034]
16. Zhao B, Schwartz LH, Jiang L, et al. Shape-constraint region growing for delineation of hepatic metastases on contrast-enhanced computed tomograph scans. Invest Radiol. 2006; 41:753–762. [PubMed: 16971799]
17. Zhou JY, Wong DW, Ding F, et al. Liver tumour segmentation using contrast-enhanced multi-detector CT data: performance benchmarking of three semiautomated methods. Eur Radiol. 2010; 20:1738–1748. [PubMed: 20157817]
18. Jung DC, Ju W, Choi HJ, et al. The validity of tumour diameter assessed by magnetic resonance imaging and gross specimen with regard to tumour volume in cervical cancer patients. Eur J Cancer. 2008; 44:1524–1528. [PubMed: 18573655]

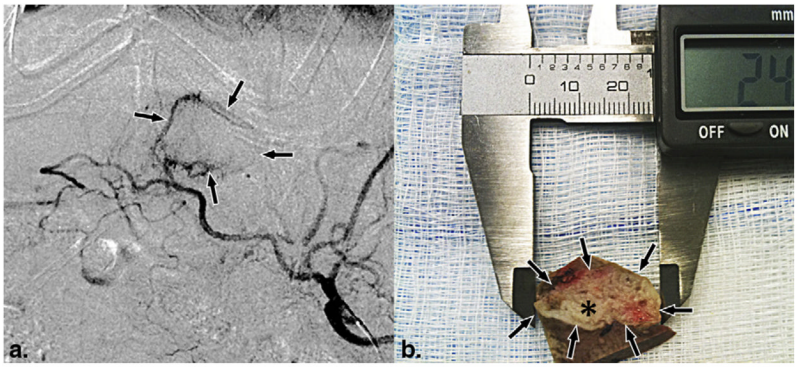

Figure 1.

(a) Selective angiogram of the common hepatic artery before embolization. VX2 tumor is located on the right lobe, fed by a hypertrophic neovessel. **(b)** Pathologic macroscopic view of a VX2 tumor (*asterisk*), with its borders indicated by *arrows*, 2 weeks after formalin fixation. This tumor was considered a prolate spheroid.

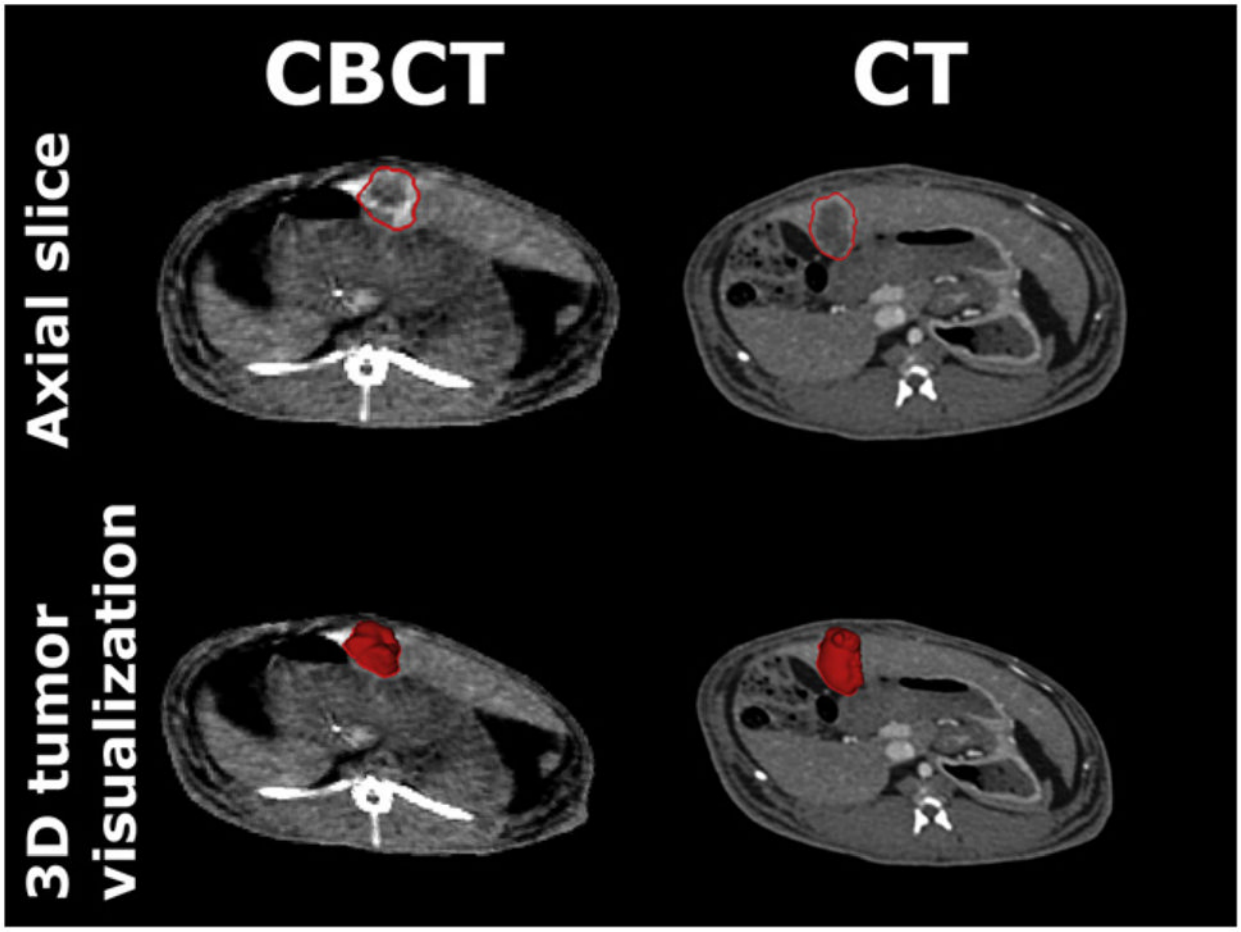

Figure 2.
Cone-beam computed tomographic (CBCT) (*left*) and multidetector computed tomographic (MDCT) (*right*) images after tumor segmentation. The *top row* shows axial slices with the tumor segmented by the “elastic band.” The *bottom row* shows the three-dimensional (3D) projected volume on a single axial slice. Note that the tumor position on CBCT and MDCT images looks slightly different. This is due to liver sliding when positioning the rabbit in two different positions on the examination table.

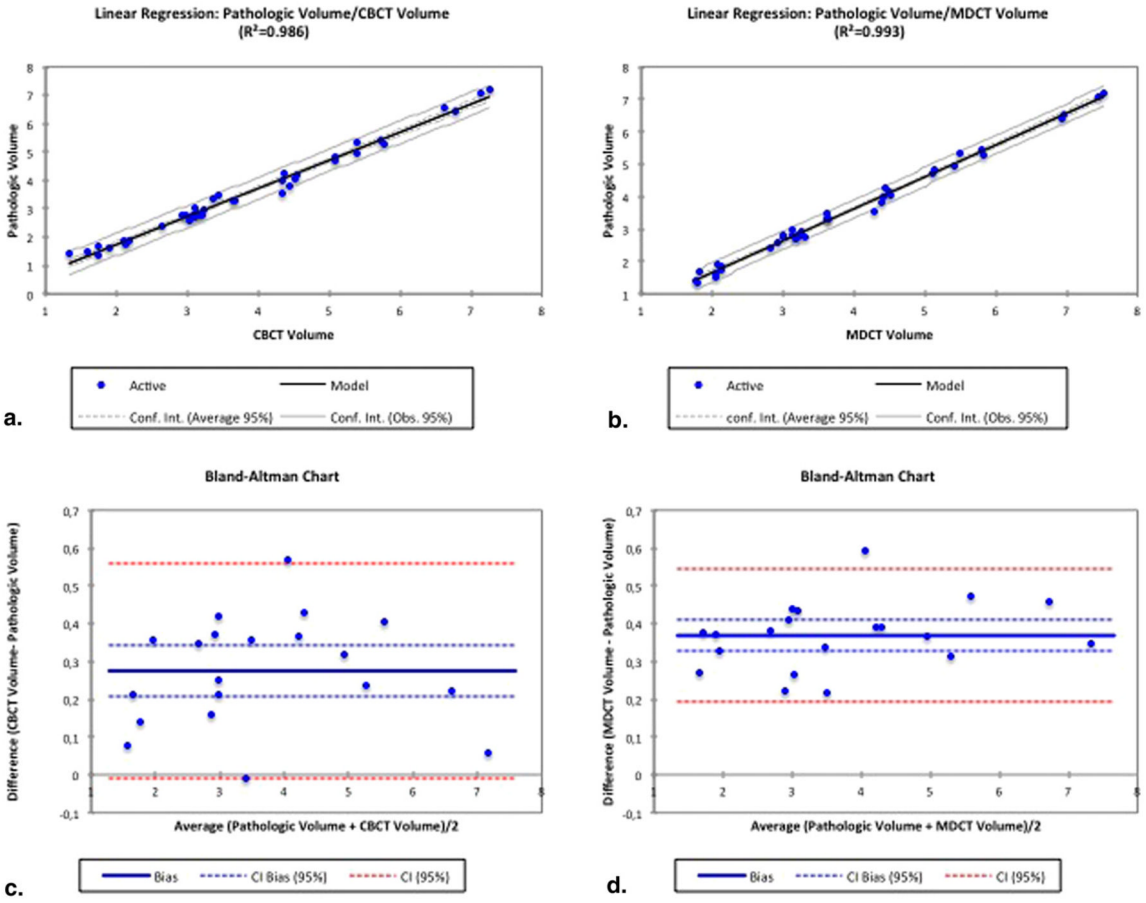

Figure 3.

Linear regression curves for tumor volume resulting from cone-beam computed tomography (CBCT) **(a)** and from multidetector computed tomography (MDCT) **(b)**. The *dotted line* represents the ideal situation of absolute agreement between the two modalities. Bland-Altman plots showing the difference against the mean for CBCT **(c)** and MDCT **(d)**. The *red dotted lines* represent the confidence interval around the mean difference.

Acad Radiol. Author manuscript; available in PMC 2013 February 18.

TABLE 1

Tumor Volume Measurements on Pathology, CBCT, and MDCT

	Pathology				Volume	
Rabbit	**Tumor Shape**	**Diameter *A* (cm)**	**Diameter *B* (cm)**	**Volume (cm^3)**	**CBCT (cm^3)**	**MDCT (cm^3)**
1	Prolate	2.2	1.1	2.79	2.92	3.21
1*		2.3	1	2.77	2.96	3.22
2	Prolate	1.7	2.3	3.48	3.43	3.61
2*		1.7	2.2	3.33	3.36	3.63
3	Prolate	1.9	0.8	1.51	1.58	2.06
3*		1.9	1	1.89	2.1	2.08
4	Prolate	2.2	2.8	7.09	7.15	7.46
4*		2.3	2.6	7.20	7.26	7.53
5	Prolate	1.4	2.7	2.77	2.98	3.32
5*		1.5	2.5	2.94	3.23	3.26
6	Oblate	1.3	3.1	6.54	6.63	6.95
6*		1.2	3.2	6.43	6.78	6.94
7	Oblate	1.6	1.3	1.42	1.32	1.76
7*		1.6	1.4	1.64	1.89	2.05
8	Oblate	1.8	1.6	2.41	2.63	2.81
8*		1.7	1.7	2.57	3.04	2.93
9	Prolate	1.8	0.8	1.36	1.73	1.79
9*		1.8	1	1.70	1.75	1.81
10	Prolate	2.5	1.3	4.25	4.36	4.43
10*		2.2	1.5	3.80	4.43	4.4
11	Oblate	1.8	1.4	1.85	2.17	2.12
11*		1.7	1.4	1.74	2.13	2.13
12	Prolate	1.6	2	2.68	3.11	3.18
12*		1.6	2.1	2.81	3.12	3.13
13	Prolate	2.1	1.2	2.77	3.22	3.01

	Pathology				Volume	
Rabbit	**Tumor Shape**	**Diameter *A* (cm)**	**Diameter *B* (cm)**	**Volume (cm^3)**	**CBCT (cm^3)**	**MDCT (cm^3)**
13*		2.2	1.1	2.79	3.18	2.99
14	Prolate	1.9	2.1	3.97	4.34	4.42
14*		1.8	2.1	3.56	4.33	4.29
15	Oblate	1.6	2.2	4.05	4.52	4.51
15*		1.8	2.1	4.16	4.55	4.48
16	Oblate	1.1	2.4	3.32	3.65	3.65
16*		1.3	2.2	3.29	3.67	3.63
17	Prolate	2.4	1.8	5.43	5.72	5.81
17*		2.3	1.9	5.26	5.78	5.82
18	Oblate	1.7	2.3	4.71	5.09	5.12
18*		1.9	2.2	4.82	5.08	5.14
19	Prolate	2.7	1.4	5.34	5.38	5.5
19*		2.6	1.4	4.95	5.39	5.42
20	Prolate	2.1	1.2	2.77	3.08	3.17
20*		2.1	1.3	3.00	3.11	3.13

CBCT, cone-beam computed tomography; MDCT, multidetector computed tomography.

*Repeated measurement in a separate session.

TABLE 2

Predictive Performance of MDCT and CBCT Using the Sheiner and Beal Method

Variable	CBCT (cm^3)	MDCT (cm^3)
Precision	0.674	0.321
Bias	0.368	0.275
Difference in precision (95% confidence interval) *	0.193–0.410	

CBCT, cone-beam computed tomography; MDCT, multidetector computed tomography.

* Difference compared to the performance of MDCT.

TABLE 3

Intraobserver Measurement Reproducibility Results, Showing Good Reproducibility of Tumor Volume Measurement by Each Method Used

Variable	Pathology	CBCT	MDCT
Average difference between two measurement (95% CI)	0.19 (0.02–0.45)	0.12 (0.01–0.57)	0.05 (0.01–0.29)
Intraclass correlation coefficient (95% CI)	0.934 (0.922–0.967)	0.951 (0.938–0.987)	0.958 (0.952–0.963)

CBCT, cone-beam computed tomography; CI, confidence interval; MDCT, multidetector computed tomography.